New measurement of the Dalitz-decay branching ratio of the π^0

M. A. Schardt*

*Department of Physics, Arizona State University, Tempe, Arizona 85281
and Los Alamos Scientific Laboratory, Los Alamos, New Mexico 87545*

J. S. Frank, C. M. Hoffman, R. E. Mischke, D. C. Moir, and P. A. Thompson[†]

Los Alamos Scientific Laboratory, Los Alamos, New Mexico 87545

(Received 26 September 1980)

An experiment measuring the Dalitz-decay branching ratio of the π^0 meson has been performed at the Clinton P. Anderson Meson Physics Facility (LAMPF). The result is $\Gamma(\pi^0 \to e^+e^-\gamma)/\Gamma(\pi^0 \to \gamma\gamma) = (1.25 \pm 0.04 \pm 0.01) \times 10^{-2}$, where the first error is due to statistics and the second is an estimate of systematic effects. This result is in agreement with the one previous high-statistics measurement and with theoretical expectations.

I. INTRODUCTION

The π^0 meson decays electromagnetically; the predominant decay mode is $\pi^0 \to \gamma\gamma$. It was first pointed out by Dalitz[1] that one of the photons could internally convert into an electron-positron pair (a Dalitz pair). This should occur with a probability $\sim \frac{1}{160}$ for a single photon or $\sim \frac{1}{80}$ for either γ from π^0 decay. The Dalitz-decay mode of the π^0 was observed in several low-statistics experiments[2-6] and the branching ratio was measured in a hydrogen bubble chamber in 1961 by Samios[7] to be

$$B = \frac{\Gamma(\pi^0 \to \gamma e^+ e^-)}{\Gamma(\pi^0 \to \gamma\gamma)} = (1.166 \pm 0.047) \times 10^{-2} . \quad (1)$$

B has been calculated in conventional quantum electromagnetic theory (QED), including radiative corrections by several authors,[8-10] yielding

$$B_{thy} = 1.196 \times 10^{-2} , \quad (2)$$

with an uncertainty[10] of less than 0.003×10^{-2}.

In an attempt to explain a discrepancy between experimental data and theoretical expectations for muonic-atom x-ray spectra, Adler, Dashen, and Treiman[11] showed that B is quite sensitive to the vacuum-polarization contribution in QED. Subsequent muonic-atom x-ray data[12] showed the earlier measurements to be incorrect. In the meantime, the prospect of testing QED helped motivate our experiment to measure B.

II. EXPERIMENTAL METHOD

A. General approach

To measure the Dalitz-decay branching ratio, it is necessary to produce π^0's and detect e^+e^- pairs which come directly from π^0 decay. Unfortunately, it is impossible to avoid a background of e^+e^- pairs from external conversions of γ's from $\pi^0 \to \gamma\gamma$ decays in the target material used to produce the π^0's. Our experimental technique eliminated this background. We also deliberately converted photons to provide a normalization. A simplified description of the method is given below.

The π^0's were produced in a CH_2 target of thickness t by the reaction $\pi^- p \to \pi^0 n$. The products of π^0 decays were detected in two arms: one arm detected a photon which was in coincidence with an electron-positron pair detected in the other. The number of π^0 Dalitz-decay events detected per incident π^- is proportional to t since the π^0 production probability is proportional to t. Thus the number of Dalitz-decay events detected per target thickness is a constant. The number of $\pi^0 \to \gamma\gamma$ events detected per incident π^- with a γ converting in the target material is proportional to t^2. The number of events per target thickness for this process extrapolates to zero at zero target thickness. Thus, extrapolating the total number of events per target thickness to zero target thickness yields a signal due only to π^0 Dalitz-decay events. The experiment was then repeated with a copper sheet in front of the pair spectrometer. The copper intercepted photons from $\pi^0 \to \gamma\gamma$ and converted a known fraction of these photons. Extrapolating the number of events per target thickness to zero target thickness for this configuration yields a signal which is the sum of that due to π^0 Dalitz-decay events and to $\pi^0 \to \gamma\gamma$ events where a photon converted in the copper sheet. Comparing the yields with and without the copper sheet results in the ratio of Dalitz-decay events to the known rate for externally converted photons from the copper sheet and, hence, B. A derivation of an approximate formula for determining B follows.

Let σ be the cross section for $\pi^- p \to \pi^0 n$, ρ be the density of protons in the target, n be the rate of incident π^-, t be the target thickness, and Ω be the acceptance of the apparatus. The detection rate for Dalitz-decay events is

$$E_D = \sigma \rho t n \Omega B . \tag{3}$$

The event rate from $\pi^0 \to \gamma\gamma$ events converting in the target is

$$E_c = \sigma \rho t n \Omega (2Kt/2) , \tag{4}$$

where the factor of 2 is due to the fact that either photon can convert, K is the conversion probability in the target per target thickness, and we assume that half of the target thickness on the average is available to convert the photon. It is also assumed here that Ω is the same for Dalitz-decay and photon-conversion events and that K is independent of photon energy. There is, in addition, a probability C_M that a photon will convert in material between the target and the detecting apparatus. The total event rate per target thickness with no copper converter is then

$$E^0/t = \sigma \rho n \Omega (B + Kt + 2C_M) . \tag{5}$$

With a copper converter in place, the event rate is increased by an amount

$$E_c^{Cu} = \sigma \rho t n \Omega (2K^{Cu} t_{Cu}) , \tag{6}$$

where K^{Cu} is the photon-conversion probability in the copper per copper thickness and t_{Cu} is the copper thickness. It is assumed that the copper sheet is large enough so as not to decrease Ω. The event rate per target thickness with a copper converter in place is

$$E^{Cu}/t = \sigma \rho n \Omega (B + Kt + 2K^{Cu} t_{Cu} + 2C_M) . \tag{7}$$

Extrapolating Eqs. (5) and (7) to zero target thickness, we find

$$I(t_{Cu}) = \sigma \rho n \Omega (B + 2K^{Cu} t_{Cu} + 2C_M) , \tag{8}$$

where $I(t_{Cu})$ is the intercept as a function of copper thickness. Defining R [in units of $(t_{Cu})^{-1}$] to be the ratio of the term proportional to t_{Cu} to the term independent of t_{Cu} in Eq. (8), we find

$$B = \frac{2K^{Cu}}{R} - 2C_M . \tag{9}$$

Even though Eq. (9) is an approximate expression it demonstrates that the determination of B depends only on the ratio of intercepts and known conversion probabilities.

B. π^0 production

The high-energy pion channel (P^3) at the Clinton P. Anderson Meson Physics Facility (LAMPF) was tuned to transport 300-MeV/c π^- mesons to the target. The beam intensity was varied from 4×10^6 π^-/s (average) to 16×10^6 π^-/s to study the dependence of the result on the instantaneous fluxes in the detectors. The π^- beam had a μ^- contamination of ~10%. Some of the muons came from pions which decayed near the production target; these

muons were transported by the channel and occupied approximately the same phase space as the pions. The rest of the muons came from pions which decayed downstream of the last bending magnet in the channel. A lead collimator was constructed just upstream of the CH_2 target to shield the apparatus from these muons. It was not necessary to measure the beam composition since B is extracted from a ratio of event rates and the only beam setting which was changed was an aperture jaw which varied the intensity but not the composition.

Three different CH_2 targets were used; the target thicknesses were (0.5936 ± 0.0017), (1.1810 ± 0.0022), and (2.370 ± 0.0025) g/cm^2. Each target was 15.2 cm wide and 7.6 cm high. The targets were much larger than the beam spot $(3 \times 3$ cm) so the experiment was insensitive to slight movements of the beam.

C. Apparatus

Figure 1 shows schematically the two arms which detected π^0 decay products. The shower counter detected photons and the large magnetic spectrometer detected electron-positron pairs. Each of these devices is discussed in more detail below.

1. Shower counter

The shower counter consisted of four scintillation counters with a 0.95-cm-thick lead sheet placed between the first and second scintillators. The first counter vetoed incident charged particles. Photons which converted in the lead sheet produced electrons and positrons which were detected in the three subsequent counters. Concident signals from all three of these counters were required by the logic. All counters were 0.64 cm thick.

The veto counter and the first two coincidence counters were each 30.5 cm wide and 61 cm high. This size was chosen to match the acceptance of the magnetic spectrometer. During the course of the experiment, we found it necessary to reduce the accidental coincidence rate between the two arms. Monte Carlo studies indicated that only ~10% of the good events counted in the 10 cm of the shower counter farthest from the beam line, while ~30% of the accidental coincidences counted there. Thus a third coincidence counter, 61 cm high but only 20 cm wide, was added to the shower counter.

2. Magnetic spectrometer

The magnetic spectrometer consisted of scintillation counters and multiwire proportional cham-

bers (MWPC's) flanking the magnet which had rectangular pole faces 86 cm wide by 44.5 cm deep, separated by a 61-cm gap. The integrated field was 8.16×10^3 G cm. The magnet was used only to separate collinear electrons and positrons so that they could be detected as two separate particles; momentum resolution was not important.

The trigger logic required coincident pulses from a scintillation counter upstream of the magnet (the G counter) and from two counters in each of two hodoscope banks located downstream of the magnet (the H and J counters). The G counter was 0.16 cm thick, 20.5 cm high, and 32 cm wide. It was located between the first two MWPC's and assured that triggering particles originated at the front of the experiment. Each of the nine H counters and nine J counters measured $1.3 \times 71.1 \times 13.8$ cm. Each H-counter scintillator was viewed by two photomultiplier tubes, one on top and one on the bottom; each J counter had only one photomultiplier. The H- and J-counter banks were separated by 2.5 cm of CH_2 to suppress neutrons registering in both banks.

The four planes of MWPC's recorded the positions of the triggering particles which passed through them. Each chamber had 20-μm-diameter goldplated tungsten signal wires, spaced 2 mm apart, in both the horizontal and vertical directions. The chamber readouts consisted of delay lines which spanned 64 signal wires. The unscattered π^- beam passed through the front two MWPC's; no position information was collected from the beam region. This design allowed the active region of the chambers to be close to the beam yet very little material was near the beam. The active areas of the first three MWPC's were 32×32, 38.4×38.4, and 70.4×51.2 cm, respectively. The fourth MWPC was actually two adjacent chambers, each 64×70.4 cm, as shown in Fig. 1.

Most of the region between the target and the first MWPC was filled with helium to minimize photon conversions in this region. The helium was contained in a box consisting of 6.4-mm-thick acrylic plates on the top and bottom, four 13-mm-diameter acrylic rods holding the plates apart, and 25-μm mylar covering the front, back, and sides.

3. Copper converters

The copper converters were placed immediately in front of the first MWPC. Each converter was 30.5 cm high and 30.5 cm wide. Monte Carlo studies were used to determine the correct size and transverse position of the converters to match the acceptance of the magnetic spectrometer. The two converters were sheets of oxygen-free copper 0.726 ± 0.003 and 1.090 ± 0.004 g/cm^2 thick, respectively.

4. Beam monitors

The data analysis required comparing runs taken under several different running conditions (target and converter thicknesses, and beam intensities). Because of the importance of knowing the incident π^- flux, four separate beam-monitoring systems were used during the experiment: an ionization chamber, an integrating scintillation counter, and two counter-telescope systems. The integrating scintillation counter consisted of a $5 \times 5 \times 0.16$-cm plastic scintillator viewed by two photomultiplier tubes, an EMI9813B and a Dumont 6292. The EMI tube produced fast pulses and was used to calibrate the integrating Dumont tube at low intensities ($\sim 2 \times 10^5$ π^-/s average). At higher intensities, the EMI tube was turned off and the current from the Dumont tube was used to measure the beam flux. This counter was located in the π^- beam, 1 m upstream of the CH_2 targets. Runs taken with no CH_2 target ("target-out" runs) showed that this counter (or any other material in the beam upstream of the target position) did not produce any background.

The scintillation plastic of the integrating counter served as a target for two separate three-counter telescopes which detected particles scattered at an angle of $\sim 80°$ relative to the beam direction.

The ionization chamber consisted of five high-voltage plates interleaved between four low-voltage signal plates and two end plates at ground potential. The end plates sealed the aluminum can which housed the chamber. The plates were made of 6-μm aluminized mylar stretched on aluminum rings. The separation between plates was 2.5 cm. The chamber was filled with argon and the 900-V high voltage was maintained by a battery. The output current was integrated and digitized.

5. Electronics and data acquisition

Fast-logic electronics required coincident pulses from the shower counter (see Sec. II C1 for the definition of a valid shower-counter pulse), two H counters, two J counters, and the G counter. The outputs from all counters were fed to CAMAC analog-to-digital converters (ADC's) and time-to-digital converters (TDC's). The signals from each end of the MWPC delay lines were amplified and fed to a discriminator. These discriminator outputs also went to CAMAC TDC's. These CAMAC modules, as well as a large number of scalers, were read out by an on-line PDP 11/45 and written onto magnetic tape for off-line analysis. For a
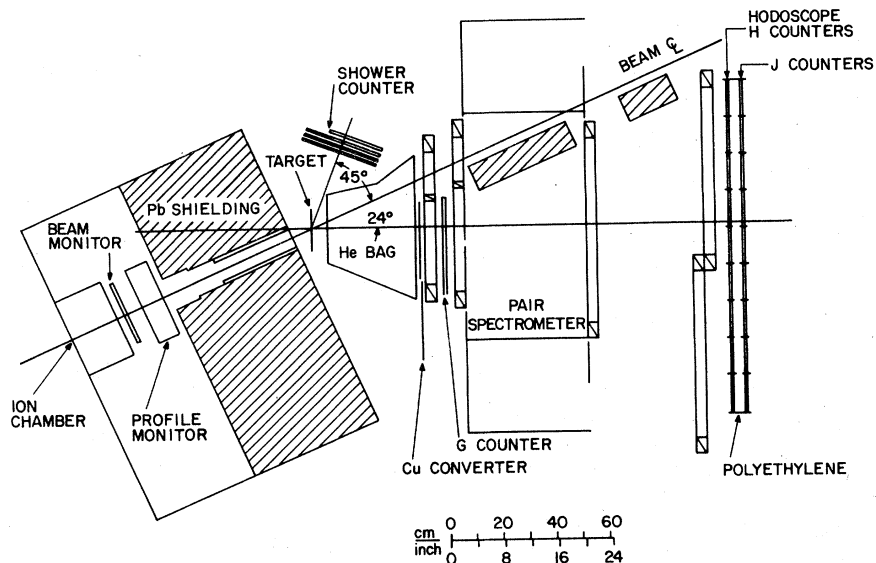
FIG. 1. Schematic view of the experimental apparatus. The MWPC's are not labeled in the figure but they can be seen flanking the pair-spectrometer magnet.

real coincident event, the time of the trigger pulse, which was used to start the TDC's, was determined by the *H*-counter pulses.

For each combination of the three target thicknesses, three copper converter configurations, and two beam intensities (4×10^6 π^-/s and 6×10^6 π^-/s), approximately 20 000 events were recorded. The events for each combination were divided into three or four separate data runs. These runs were randomly distributed in time to minimize the effects of any drifts in the performance of the apparatus.

III. DATA ANALYSIS

A. Event selection

Each event was subjected to a series of tests designed to eliminate invalid events from the data sample. Several cuts were imposed to assure that the event originated from the target area. The most important cut was to require the event to have produced a signal in the active region of both planes of the first MWPC and that the tracks passed through the *G* counter. This cut eliminated events in which the photon converted in either the *G* counter or the frame of the first chamber. Corrections for photon conversions in the material upstream of the active region of the first chamber and for chamber inefficiencies are discussed below.

Additional cuts required signals in at least two out of the three remaining MWPC's in each of the two projections, and agreement between the track extrapolations and the *H* and *J* counters which

fired and with the target position.

The percentage of triggers eliminated by these cuts varied according to the experimental configuration. Table I shows the percentage of triggers surviving all previous cuts, failing each cut for runs with the 1.19-g/cm^2 target, no copper converter, and a beam intensity of 6×10^6 π^-/s.

B. Corrections to the data

The number of events must be corrected for effects due to apparatus inefficiencies (especially chamber one), accidental counts in the trigger, and dead time to the data acquisition system at high event rates.

1. Chamber inefficiencies

The chamber inefficiencies were primarily due to dead time in the MWPC readout electronics. The true chamber efficiencies were measured in separate runs at low rates by placing several scintillation counters on each side of a chamber. The chamber efficiencies measured in these runs were typically greater than 98%. The effective chamber efficiency including effects from electronic dead time had to be determined from the data of each run.

In principle, the effective efficiency of a chamber plane could be established by counting how often that plane fired when all other chamber planes fired. This method was found to yield the correct efficiency for all chambers except for the first MWPC. The first MWPC had singles rates which depended strongly on whether or not a copper

TABLE I. Percentage of triggers failing cut.

Cut	Percentage
Signal in first MWPC	18.6
Fiducial region of first MWPC	5.1
Signals in at least 3 of 4 MWPC's	1.3
H, J counters agree with tracks	1.4

converter was in place. The copper tended to shield the chamber from low-energy particles produced in the target. Some valid triggers resulted from photons converting in the material of the first MWPC. The percentage of this kind of event also depended on whether or not a copper converter was in place.

The correction for the first MWPC was made by relating the effective efficiency, as measured above, to the G-counter singles rate which reflects the true singles rate in the chamber. The effective efficiency was measured to be a unique function of the singles rate for a given copper-converter status, regardless of incident π^- intensity or target thickness. However, as shown in Fig. 2, it is systematically several percent lower for data taken with no converter compared with data taken with a converter, as expected. This is due to the difference in the percentage of triggers in which a photon converts in the G counter for different copper configurations. Since the measured branching ratio depends on ratios of event rates, it is unnecessary to know the true efficiency of chamber one. The correction due to the efficiencies of other chambers is much less critical since they are much weaker functions of the experimental configuration and because the cut allowed one of the last three X planes and one of the last three Y planes to be missing. Figure 2 indicates the size of the chamber-one correction. The total correction due to the other chambers was typically 0.1%.
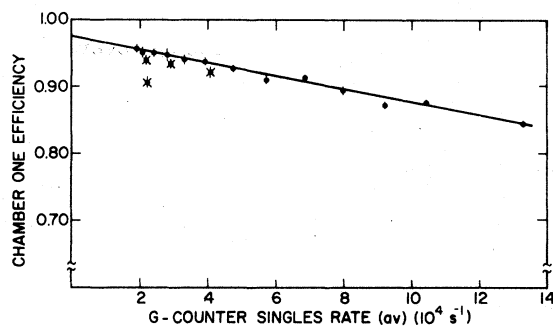
FIG. 2. Efficiency of the first MWPC versus the G-counter singles rate. The dots show data taken with a copper converter in place; the crosses show data with no copper converter.

2. G-counter correction

A G-counter signal was required as part of the fast logic. However, the particle which passed through the G counter could have been in accidental coincidence with the particles which hit the H and J counters. A correction had to be made to account for the accidental G-counter pulses. This correction was made by comparing the number of events in the true coincidence peak in the G-counter timing spectrum to the number of events outside this peak. The correction for accidental coincidences ranged between 0.2 and 2.3%.

3. Shower-counter correction

A correction had to be made to account for the accidental vetoes of good signals in the shower counter by the veto counter. This correction was made from the measured veto-counter singles rate and the length of the veto signal, and typically differed from unity by 1 to 2%.

4. Random-coincidence correction

A correction was made for the random coincidences between the magnetic-spectrometer arm and the shower-counter arm. The correction was essentially the ratio of accidental coincidences to the number of triggers, where the accidental coincidences were measured by delaying the shower-counter pulses by ~80 ns and scaling the number of coincidences. It is possible that a higher percentage of the accidental coincidences than the in-time triggers would have been eliminated by the cuts. To study this effect, several runs under varying experimental conditions were taken with accidental coincidences triggering the apparatus. The final correction due to random coincidences ranged from 1 to 3%.

5. Computer dead time

The final correction to the data was due to dead time introduced while the data acquisition computer was reading out the CAMAC modules. This correction was based on the ratio of two scalers, one gated off by the computer when it was busy and the other ungated. This correction was generally smaller than 1%.

C. Beam monitors

A crucial aspect of the analysis of the data was the determination of the relative beam intensity for each data run. The beam monitors described above were compared against each other to verify their stability and linearity. The ionization chamber and the integrating scintillation counter ex-

hibited both long- and short-term drifts relative to the other monitors and so they were not used in the final analysis. It was found that the shower counter was a very stable beam monitor for a given target thickness so it was used in the determination of the relative π^- flux for each data run. The data from the three monitors (the two counter telescopes and the shower counter) were combined to form a total monitor.[13] The relative weighting of each individual monitor was determined from the data set and was independent of experimental conditions except for a linear dependence of the shower-counter rate on target thickness. The relative weights of each monitor for each data run were checked for consistency with the weights determined from the entire data set. Several runs were discarded due to inconsistent monitors. The total monitor was found to be independent of target and copper-converter thickness.

IV. MONTE CARLO CALCULATION

Equations (3)–(9) are not exact because they do not take into account the difference in the acceptance of the apparatus for π^0 Dalitz-decay events and $\pi^0 \to \gamma\gamma$ events with a photon converting in either the target or a copper converter, the variation of the acceptance with target thickness or copper-converter thickness, or the energy dependence of the photon-conversion probability in the target and in the copper converters. A Monte Carlo calculation was required to take account of all of these effects.

The code started with a π^- beam with momentum, spatial, and angular distributions corresponding to the measured distributions of the beam. The momentum and direction of the π^0 were selected according to the published $\pi^0 p \to \pi^0 n$ cross sections.[14]

For the Dalitz-decay mode, the distributions in the electron-positron effective-mass squared

$$X^2 = (E_+ + E_-)^2 - (\vec{P}_+ + \vec{P}_-)^2 \tag{10}$$

and the energy partition

$$Y = (E_+ - E_-)/|\vec{P}_+ + \vec{P}_-| \tag{11}$$

were taken from the detailed QED calculations with radiative corrections.[9,10]

Once the Dalitz decay had been simulated in the target, the decay products ($\gamma e^+ e^-$) were transported through the apparatus. The photon was followed first to see if it struck and converted in the lead sheet of the shower counter. Energy-dependent conversion probabilities were calculated from the method outlined by Tsai.[15]

If the photon successfully converted in the shower counter, the leptons were traced through the mag-

netic spectrometer. The leptons were first propagated through the remaining target material. Ionization loss, multiple scattering, and bremsstrahlung were carefully simulated whenever lepton trajectories encountered material. The leptons were then traced to the plane of the copper converter. If a converter was present, ionization loss, multiple scattering, and bremsstrahlung were again taken into account. After traversing the converter, the leptons were propagated through the magnet and the MWPC's to the H- and J-counter banks. The intersection points with the chambers and scintillation counters were recorded and cuts were made to simulate the requirements of the data analysis code.

Figure 3 shows the X distribution for all Dalitz-decay events and for those accepted by the apparatus. It can be seen that the apparatus is most efficient for events with small X.

The transport of the photons from $\pi^0 \to \gamma\gamma$ began similarly to the transport of the products of the Dalitz-decay events. One photon was required to "trigger" the shower counter while the second photon converted in the target or the copper converter (if present). The energy-sharing distribution and the angular distribution for the leptons from pair production were taken from Rossi.[16] Once the leptons were produced, the program proceeded as for the Dalitz-decay events.

For each combination of target thickness and copper-converter thickness, the acceptance for Dalitz-decay events, and for $\pi^0 \to \gamma\gamma$ events with the photon converting in the target and in the copper converter (if present) were each found. The total event rate for each apparatus configuration is obtained by summing the individual rates, as in Eqs. (5) and (7). This method takes into account the change in acceptance caused by the added material introduced by changing the target or converter thickness.

The results of the Monte Carlo calculation, assuming $B = 1.2 \times 10^{-2}$, are shown in Fig. 4, plotted as a function of target thickness. These results
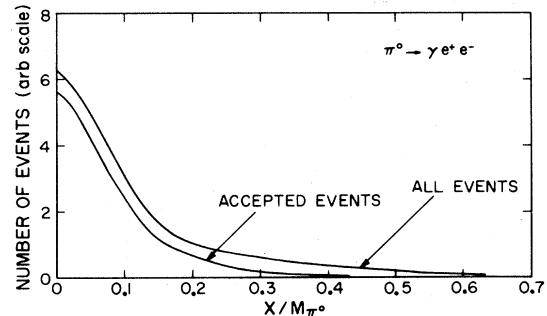
FIG. 3. The number of events versus X/M_{π^0} for Dalitz decay. The results are from Monte Carlo calculations.
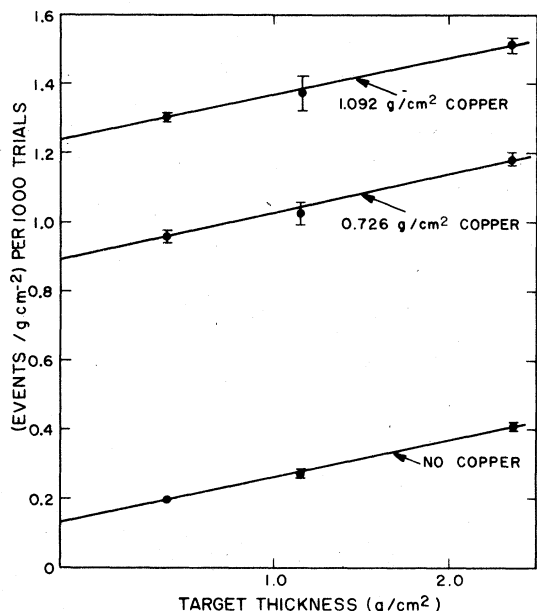
FIG. 4. Monte Carlo yields versus target thickness. The number of accepted events per target thickness per 1000 attempts is plotted against target thickness from the Monte Carlo simulation.

are fit quite well by a straight line as a function of target thickness, as expected from Eqs. (5) and (7). The errors shown are statistical uncertainties in the Monte Carlo calculation.

Least-squares fits to the results as a function of target thickness yield the intercepts shown in Table II. Also shown are the intercepts for $B = 1.1 \times 10^{-2}$ and 1.3×10^{-2}.

V. RESULTS AND CONCLUSIONS

A. Results

The method of event selection and the corrections which must be applied to the measured event rates were discussed in Sec. III. The number of corrected events per target thickness for each run was normalized to the combined beam-monitor signal. In order to study the rate dependence of the yields and corrections, some runs were taken at π^- intensities of 9×10^6 π^-/s and 16×10^6 π^-/s. The corrected yields were found to be insensitive to the instantaneous rates. These data sets were not included in the final analysis because of a raw

TABLE II. Intercepts—Monte Carlo [in (events/ g cm^{-2}) per 1000 trials].

	I^0	I^{C_1}	I^{C_2}
$B = 1.1 \times 10^{-2}$	1.208 ± 0.023	8.78 ± 0.22	12.26 ± 0.20
$B = 1.2 \times 10^{-2}$	1.292 ± 0.024	8.84 ± 0.22	12.33 ± 0.20
$B = 1.3 \times 10^{-2}$	1.381 ± 0.025	8.93 ± 0.22	12.41 ± 0.20

trigger rate-dependent problem in the data acquisition system which affected some combinations of target thickness and Cu-converter runs.

Figure 5 shows the corrected event rates per target thickness for incident π^- intensities of 4×10^6 π^-/s and 6×10^6 π^-/s. These data show no significant dependence on beam intensity and are in good qualitative agreement with the Monte Carlo results of Fig. 4. The data and the Monte Carlo results do disagree somewhat on the ratio of the slope to intercept for the data with copper converters in place. This is presumably due to some process which is proportional to some higher power of t which is not adequately calculated in the Monte Carlo program. The contribution from such higher-order processes disappears in the extrapolation to zero target thickness. A least-squares fit to the data yields the intercepts shown in Table III. It is unimportant that the units are different for the intercepts of the data and the Monte Carlo results, since it is only the ratio of intercepts that is important [see Eq. (9)].

In order to extract the Dalitz-decay branching ratio B from the intercepts, the intercepts of Tables II and III are fit to linear functions of the copper-converter thickness as in Eq. (8). The ratio R, defined in Sec. IIA, is shown in Fig. 6 for the data and for the Monte Carlo results as a function of B. Comparing the Monte Carlo results with the data,

$$B = \frac{\Gamma(\pi^0 \to \gamma e^+ e^-)}{\Gamma(\pi^0 \to \gamma\gamma)} = (1.25 \pm 0.04) \times 10^{-2}, \qquad (12)$$

where the errors are statistical only (due to the statistical errors in both the data and the Monte Carlo calculation).

B. Systematic errors

There are several sources of possible systematic errors which are discussed below and sum-

TABLE III. Intercepts—data [in (events/g cm^{-2}) per beam monitor].

Beam intensity $(10^6 \, \pi^-/s)$	I^0	I^{C_1}	I^{C_2}
4	0.1995 ± 0.0061	1.362 ± 0.025	1.845 ± 0.035
6	0.2015 ± 0.0058	1.358 ± 0.024	1.833 ± 0.030
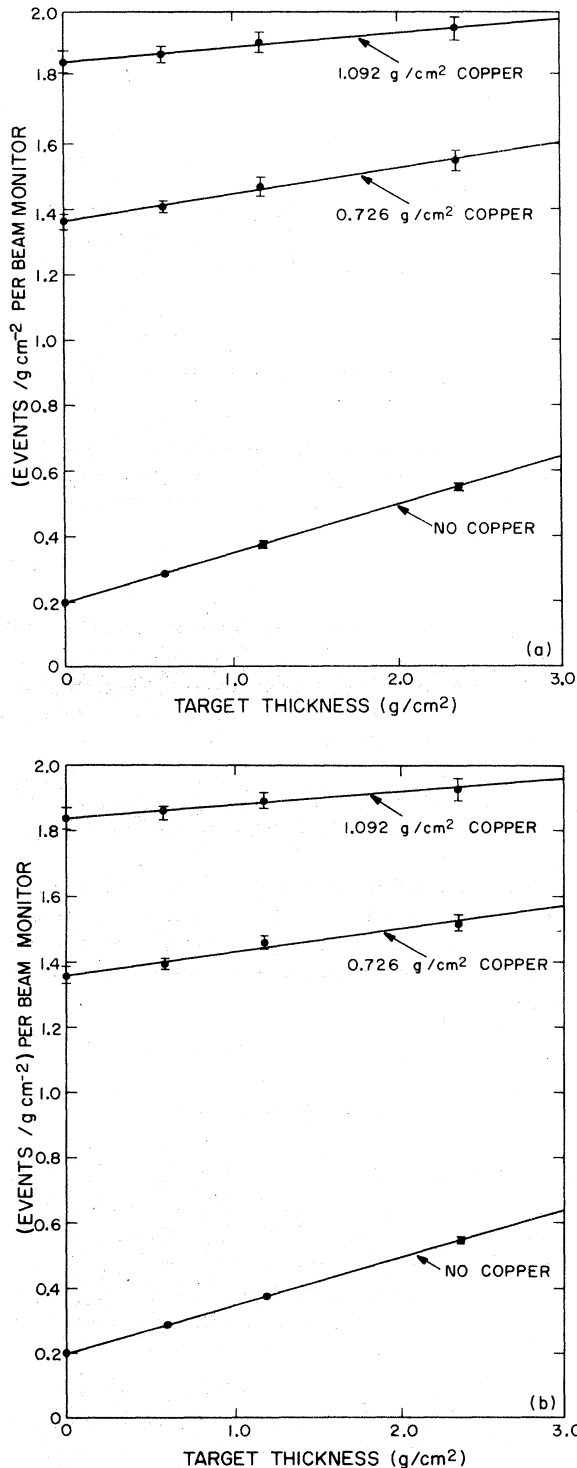
FIG. 5. (a) The corrected number of events per target thickness per beam monitor is plotted versus target thickness for the beam intensity of $4 \times 10^6 \ \pi^-/s$. The three curves are least-square fits for the no-copper, thin-copper, and thick-copper configurations of the experiment. (b) Normalized yield versus target thickness of $6 \times 10^6 \ \pi^-/s$ beam intensity.

marized in Table IV.

Since the extraction of the branching ratio involves extrapolating the yields per target thickness to zero target thickness, the determination of B depends upon the knowledge of the target thickness. The thickness and density of each target was carefully measured so that the uncertainty in the thickness of each target was ~0.002 g/cm². By analyzing the data as a function of target thickness, the uncertainty in the target thicknesses results in an uncertainty in B of $\pm 0.002 \times 10^{-2}$.

The uncertainty in the copper-converter thicknesses results in an uncertainty in B of $\pm 0.004 \times 10^{-2}$.

Material between the target and the first MWPC can convert photons and result in an event yield per target thickness which is approximately constant. These events were included in the Monte Carlo calculation of the expected yields for each experimental configuration. The material includes air, helium, the windows of the helium box, and the window and some gas in the first MWPC. The uncertainties in the amounts of each of these materials implies an uncertainty in B of $\pm 0.002 \times 10^{-2}$.

The effects of strong interactions at the π^0 virtual-photon vertex can be taken into account by a form factor F which is a function of the virtual-photon invariant mass X. The effect of this form factor has been considered by several authors[11,17] assuming vector-meson dominance and is expected to contribute ~0.2% to B. The form factor is expected to vary slowly in the kinematically allowed range of X $(2M_e < X < M_{\pi^0})$ and is usually approximated by the linear expansion

$$F(X) = 1 + a(X/M_{\pi^0})^2 . \tag{13}$$

A recent measurement by Fischer *et al.*[17] of the form factor yielded $a = 0.11 \pm 0.03$, which is somewhat higher than the vector-meson-dominance expectation of $a \simeq 0.03$.

The experimental uncertainty in the slope of the π^0 form factor results in an uncertainty in the measurement of B since the apparatus acceptance is a strong function of X (see Fig. 3). The resulting error in B is $\pm 0.001 \times 10^{-2}$. Taking $a = 0.03$ would increase B by 0.002×10^{-2}.

The largest systematic uncertainty is due to the uncertainty in the absolute photon-conversion probability in copper. We have assumed a theoretical uncertainty in the conversion probability of $\pm 1\%$ (Ref. 16) which results in an uncertainty in B of $\pm 0.013 \times 10^{-2}$. A list of the systematic errors is given in Table IV. Combining all of the systematic errors in quadrature, the total systematic error is 0.014×10^{-2}.

TABLE IV. Systematic errors.

Quantity	Error in branching ratio
Target thickness	0.002×10^{-2}
Copper-converter thickness	0.004×10^{-2}
Absolute copper-conversion probability	0.013×10^{-2}
Material between target and first MWPC	0.002×10^{-2}
π^0 form-factor slope	0.001×10^{-2}

C. Backgrounds

Several background processes have been considered that would require detection of a neutron in the shower counter. These processes are

$$\pi^- p \to n\gamma , \qquad (14a)$$

$$\pi^- p \to n e^+ e^- , \qquad (14b)$$

$$\pi^- p \to n\pi^0 \qquad , \qquad (14c)$$
$$\quad\searrow \gamma\gamma$$
$$\qquad\searrow \gamma e^+ e^-$$

$$\pi^- p \to n\pi^0 \qquad . \qquad (14d)$$
$$\quad\searrow e^+ e^-$$

These processes can be neglected because the neutron detection efficiency is small and the cross section for these processes [except for Eq. (14c)] is low. If every neutron which underwent charge-exchange scattering in the lead sheet were detected, the neutron detection efficiency in the shower counter would be <10%. It is unlikely that the charged products of the neutron interaction would penetrate three 0.64-cm-thick counters. The processes in Eq. (14c) will contribute to the π^0 Dalitz-decay signal while (14a) will be eliminated by the extrapolation technique. The other two processes contribute to the event rate at a level much less than 1% of the rate from π^0 Dalitz decay.

D. Conclusion

The final result is

$$B = (1.25 \pm 0.04 \pm 0.01) \times 10^{-2} , \qquad (15)$$
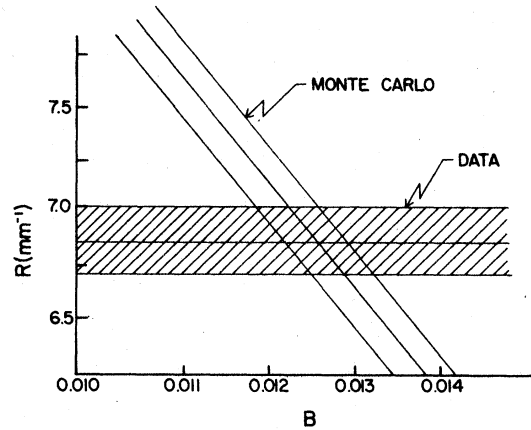
FIG. 6. The ratio R, defined in Sec. IIA, versus the Dalitz-decay branching ratio B for the data and for the Monte Carlo results. The bands correspond to 1 standard deviation.

where the first error is statistical and the second is systematic. This result is consistent with the previously reported result of Eq. (1), (1.166 $\pm 0.047) \times 10^{-2}$. A weighted average of the two experimental results gives

$$B = (1.21 \pm 0.03) \times 10^{-2} . \qquad (16)$$

This result is in agreement with the QED calculation [Eq. (2)].

The dominant uncertainty in this experiment is due to the limited counting statistics. The technique appears capable of yielding a more accurate result if substantially more events could be collected.

*Present address: Siemens Gammasonics Inc., Des Plaines, Illinois 60018.

†Present address: Brookhaven National Laboratory, Upton, New York, 11973.

[1] R. H. Dalitz, Proc. Phys. Soc. London A64, 667 (1961).

[2] R. A. Daniel, J. H. Davies, J. H. Mulvey, and D. H. Perkins, Philos. Mag. 43, 753 (1952).

[3] J. Lord, J. Fainberg, D. Haskin, and M. Schein, Phys. Rev. 87, 538 (1952).

[4] B. M. Anand, Proc. Phys. Soc. London A220, 183 (1953).

[5] P. Lindenfeld, A. Sachs, and J. Steinberger, Phys. Rev. 89, 531 (1953).

[6] C. Sargent, R. Cornelius, M. Rinehart, L. M. Leder-

man, and M. Rogers, Phys. Rev. <u>98</u>, 1349 (1955).

[7]N. P. Samios, Phys. Rev. <u>121</u>, 275 (1961).

[8]N. M. Kroll and W. Wada, Phys. Rev. <u>98</u>, 1355 (1955).

[9]D. W. Joseph, Nuovo Cimento <u>16</u>, 997 (1960).

[10]B. E. Lautrup and J. Smith, Phys. Rev. D <u>3</u>, 1122 (1971); K. O. Mikaelian and J. Smith, Phys. Rev. D <u>5</u>, 1763 (1972).

[11]S. L. Adler, R. I. Dashen, and S. B. Treiman, Phys. Rev. D <u>10</u>, 3728 (1974).

[12]M. X. Dixit *et al.*, Phys. Rev. Lett. <u>35</u>, 1633 (1975).

[13]T. J. Devlin *et al.*, Phys. Rev. D <u>8</u>, 136 (1973).

[14]E. Garwin, W. J. Kernan, C. O. Kim, and C. M. York, Phys. Rev. <u>115</u>, 1295 (1959).

[15]Y. Tsai, Rev. Mod. Phys. <u>46</u>, 815 (1974) and private communication.

[16]B. Rossi, *High Energy Particles* (Prentice-Hall, New York, 1952).

[17]H. Kobrak, Nuovo Cimento <u>20</u>, 1115 (1961); S. Devons *et al.*, Phys. Rev. <u>184</u>, 1355 (1969); J. Fischer *et al.*, Phys. Lett. <u>73B</u>, 359 (1978).